24

Microwave Remote Sensing of Soil Moisture in Semi-arid Environment

A. K. M. Azad Hossain and Greg Easson
The University of Mississippi
United States of America

1. Introduction

Soil moisture, defined as the water content in the upper layer of soil, is the hydrologic variable that controls the interactions (and feedbacks) between land surface and atmospheric processes (Hossain and Anagnostou, 2005). Soil moisture is important in the distribution of precipitation between runoff and infiltration (Baghdadi et al., 2006). Soil moisture monitoring and characterization of the spatial and temporal variability of soil moisture at scales from small catchments to large river basins is important in the understanding of subsurface – land surface – atmospheric interactions as well as, drought analysis, crop yield forecasting, irrigation planning, flood protection, and forest fire prevention (Georgakakos and Baumer, 1996; Robock et al., 2003). Surface soil moisture distribution information is a critical forcing variable in many Soil Vegetation Atmosphere Transfer (SVAT) models to estimate profile soil moisture at daily time steps. Soil moisture distribution also plays a key role in the prediction of erosion and sediment loads in watershed streams and ponds. In arid and semi-arid watersheds soil moisture content has been used as a surrogate indicator of general plant health (Moran et al., 2004).

Research in the extraction of soil surface moisture information from remotely sensed imagery has been an important research topic in the last decade. Optical remote sensing data have been used successfully for mapping and monitoring relative variations in soil moisture when reflective data are combined with thermal data from the same sensors (e.g., Carlson et al., 1995; Lambin and Ehrlich, 1996; Gillies et al., 1997; Hossain and Easson, 2008 & 2006). Microwave remote sensing techniques provide a direct measurement of the surface soil moisture for a range of vegetation cover conditions within reasonable error bounds (Jackson, 2002). Passive microwave remote sensing uses radiometers that detect and measure the natural thermal microwave emissions of a particular frequency, within a narrow band. This measurement provides the brightness temperature, which includes contributions from the atmosphere, reflected sky radiation, and the land surface. The Advanced Microwave Scanning Radiometer - Earth Observing System (AMSR-E) sensor on NASA's Aqua satellite and the Soil Moisture and Ocean Salinity (SMOS) mission of European Space Agency (ESA) are the two major currently operating passive microwave sensors dedicated to soil moisture mapping. Active microwave sensors produce energy and

measure the amount of energy returned from the target to yield a variable called the backscattering coefficient (σ^o or β^o). The backscattering coefficient is related to the surface reflectivity, which is used to determine surface soil moisture (Ulaby et al., 1986). Radarsat 2 Synthetic Aperture Radar (SAR), ENVISAT Advance Synthetic Aperture Radar (ASAR) and Advanced Land Observing Satellite (ALOS) Phased Array Type L-band Synthetic Aperture Radar (PALSAR) are the most widely used currently operating spaceborne active microwave sensors.

This chapter provides a brief overview of active microwave soil moisture remote sensing and presents a case study of soil moisture mapping in a semi-arid environment. The overview of active microwave soil moisture remote sensing includes a discussion of the basic principles of microwave remote sensing emphasizing soil surface moisture information extraction and different methods for soil moisture estimation using SAR data with emphasis on the existing algorithms for SAR based soil moisture mapping in semi-arid environment. The case study presents research in southeastern New Mexico that explored the linear and the non-linear relationships between radar reflectivity (backscatter) and soil moisture and determined the impact of vegetation in soil moisture estimation.

1.1 Basic Principles of Synthetic Aperture Radar (SAR)

RADAR (RAdio Detection And Ranging) sensors operate in the microwave portion of the electromagnetic spectrum beyond the visible and thermal infrared regions. Imaging radars are generally considered to include wavelengths from 1 mm to 1 m. RADAR is an active sensor, transmitting a signal of electromagnetic energy, illuminating the terrain, and recording or measuring the response returned from the target or surface. Thus, the term "active microwave" is often synonymous with radar (Henderson and Lewis, 1998). As an active sensor, radars are independent of the sun and sun conditions and can operate day or night. Radar can, in effect, collect data on a 24 hour basis. Unlike optical sensors, imaging radars are not affected by cloud or haze and operate generally independent of weather conditions.

SAR

Traditionally (before 1978) radar imaging was conducted using Real Aperture Radar (RAR) systems. RAR transmits a narrow angle beam of pulse radio wave in the range direction at right angles to the flight direction (called the azimuth direction) and receives the backscatter from the targets, which is transformed into a radar image from the received signal. Aperture is the opening used to collect the reflected energy used to form an image. In the case of radar imaging the aperture is the antenna and for RAR systems, only the amplitude of each echo return is measured and processed. The spatial resolution of a RAR system is mainly determined by the size of the antenna. For any given wavelength, the larger the antenna the better the spatial resolution. It is difficult to attach large antenna to aircraft or spaceborne sensor systems. For example a 1 km diameter antenna is needed in order to obtain 25 m resolution with L band (λ=25 cm) at a distance of 100 km from a target.

In order to overcome this limitation, radar systems with a synthetic aperture have been developed, which simulate an artificial (or virtual) antenna. Synthetic Aperture Radar (SAR) takes advantage of the Doppler history of the radar echoes generated by the forward motion

of the spacecraft to synthesize a large antenna, enabling high azimuthal resolution in the resulting image using a physically small antenna and longer radar wavelength.

Active Microwave Region in EMS

The microwave portion of the Electromagnetic Spectrum (EMS) is large, relative to the visible, and there are several wavelength ranges or bands used in radar imaging. Imaging radar systems operate at specific wavelengths or frequencies in the EMS. The active microwave regions include X, C, L and K band, which refers to specific segments of the microwave portion of the EMS. For example, an X band system would be radar that operates at a single wavelength within this band (e.g., 3.2 cm) (Henderson and Lewis, 1998). Most of the spaceborne radar systems operate in C (5.7 cm) and L (24 cm) bands.

Radar Imaging Geometry

Interpretation of SAR imagery for information extraction requires an understanding of radar imaging geometry, the nature of interaction between radar energy and surface features, and the parameters used to characterize the performance of different SAR systems. Figure 1 is a schematic diagram that illustrates the geometry of radar imaging and related radar terminology. In radar imaging systems, the platform (a) travels forward in the flight direction (b) with the nadir point (c) directly beneath the platform. The microwave beam (k) is transmitted obliquely at right angles to the direction of flight, illuminating a swath (usually the width of the imaging area) (f), which is offset from nadir. Range (e) refers to the across-track dimension perpendicular to the flight direction (b), while azimuth (d) refers to the along-track dimension parallel to the flight direction (b). Near range (h) is the portion of the imaging swath closest to the nadir track and far range (g) is the portion of the imaging swath farthest from the nadir track. Depression angle (α) is the angle between the horizontal and a radar ray path. Slant range distance (i) is the radial line of sight distance between the radar and each target on the surface. Ground range distance is the true horizontal distance along the ground corresponding to each point measured in slant range. Incidence angle (θ) is the angle between the radar beam and the perpendicular to the ground surface. Look angle (β) is the angle at which the radar looks at the surface, or the angle between vertical and the ray path.

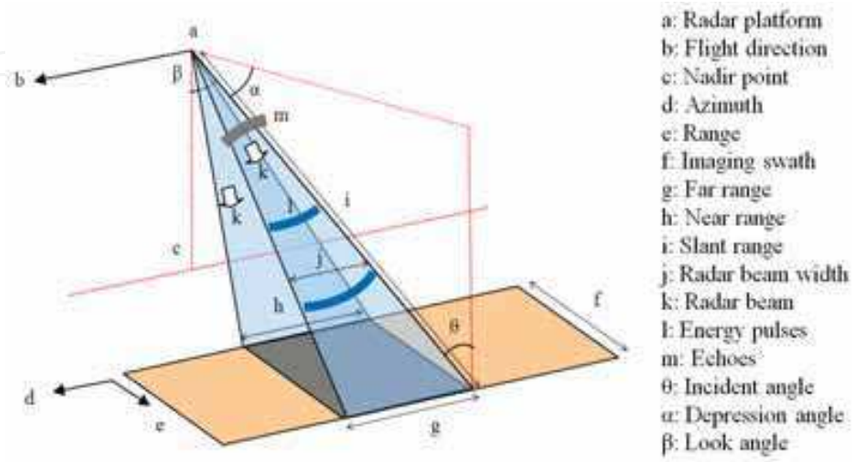

Fig. 1. Radar imaging geometry (adopted from Henderson and Lewis, 1998).

Target Interaction

In active microwave system, the energy received by a radar derives from one or more individual reflections. In a typical scene, there are many scatterers contributing to the energy received from a given region, and the locations of the individual scatterers are random (not necessarily maintaining any pattern). Usually the net signal for the scene is described by using an average over the region, leading to a distributed or diffuse scatterer model (Raney, 1998). In active systems, the brightness or darkness of the image is dependent on the amount of the transmitted energy that is returned back to the radar from targets on the surface as a measure of reflectivity (backscatter). Bright areas are produced by strong radar responses and darker areas are from weaker radar responses. Sigma-naught (σ^o) is commonly used to describe the average reflectivity or scattering co-efficient of a radar scene. Beta-naught (β^o) interprets the brightness estimates of mean reflectivity. Beta-naught (β^o) separates the radiometric response and reflectivity dependent on the terrain properties, such as local slope. According to Glen and Carr (2004):

$$\sigma^o = \beta^o + 10\log_{10}(\sin l) \quad (1)$$

$$\beta^o = 10\log_{10}(DN^2 + A_3 / A_2) \quad (2)$$

Where, DN = Digital number, A_3 = fixed offset from the radiometric data record, A_2 = look-up table (LUT) value, and l = local incidence angle.

Beta-naught (β^o) is suggested as standard terminology for the output product of most imaging radars (Raney, 1998).

Response to radar energy (for a given wavelength and polarization) by the target is primarily dependent on three factors: surface roughness, local incident angle and the dielectric constant of the target materials (Raney, 1998). Surface Roughness is measured as the average height variation in the surface cover (measured in cm). Rayleigh (1945) proposed that the criterion for roughness depended on three parameters; incident angle, wavelength and surface irregularities. A surface is considered smooth if the height variations are smaller than the radar wavelength. Specular reflection is caused by a smooth surface where the incident energy is reflected and not backscattered. This results in smooth surfaces appearing as darker toned areas on an image. Diffuse reflection is caused by a rough surface, which scatters the energy equally in all directions. A significant portion of the energy will be backscattered to the radar, such that a rough surface will appear lighter in tone on an image.

Corner reflection occurs when the target object reflects most of the energy directly back to the antenna resulting in a very bright appearance to the object. This occurs where there are buildings, metallic structures (urban environments) and cliff faces, folded rock (natural environments).

Image geometry and radiometry are influenced by the angle of the incident illumination with respect to the local slope of the scene towards the radar. The image brightness per pixel is sensitive to the local incident angle, however, variations in the aspect angle due to the component of slope in the azimuth direction has negligible impact on image brightness (Guindon, 1990). Maxwell's formulation considered the propagation of electromagnetic

waves through media characterized by certain physical constants, one of which is the dielectric constant. The dielectric constant (or the complex permittivity) is the principal description of the medium's response to the presence of an electrical field (Raney, 1998). The dielectric constant is measured as the ratio of the permittivity of a substance to the permittivity of free space. The material's dielectric constant depends weakly on frequency, but its loss tangent depends strongly on frequency (Raney, 1998).

System Parameters

Along with wavelength (or frequency), polarization and resolution are the two most important system parameters that are used to interpret the performance of an imaging radar system. Polarization of the radar signal is the orientation of the electromagnetic field and is a significant factor by which the radar signal interacts with objects on the ground, reflecting back the resulting energy. Most radar imaging sensors are designed to transmit microwave radiation either horizontally polarized (H) or vertically polarized (V), and receive either the horizontally or vertically polarized backscattered energy. Polarizing radar has four possible combinations of both transmit and receive polarizations: HH - for horizontal transmit and horizontal receive, VV - for vertical transmit and vertical receive, HV - for horizontal transmit and vertical receive, (cross-polarized), VH - for vertical transmit and horizontal receive (cross-polarized). The spatial resolution of a radar system is the ability to distinguish between different objects, and it is dependent on the properties of the microwave radiation and geometric effects. There are two types of spatial or ground resolution: range resolution (across-track resolution) and azimuth resolution (along-track resolution). Range resolution requires that the objects be separated by more than half the pulse length. Azimuth resolution is dependent on the angular width of the radiated microwave beam and the slant range distance. The azimuth resolution becomes more coarse with increasing distance from the sensor. More detail discussion on the imaging radar's system parameters can be found in Henderson and Lewis (1998). Table 1. shows the system parameters of commonly used radar imaging systems.

System parameters	Radarsat 1/2 SAR	ERS SAR	ENVISAT ASAR	ALOS PALSAR
Incidence angle (°)	20-50	23	15-45	10-51
SAR Band	C	C	C	L
Wavelength (cm)	5.7	5.7	5.7	23
Polarization	HH	VV	HH, VV, VH, HV	HH, VV, VH, HV
Resolution (m)	3-100	30	10-100	10-100
Repeat pass	24	35	35	46

Table 1 System parameters of different SAR platforms

1.2 Estimation of Soil Moisture Using SAR

Measuring and mapping soil moisture has been investigated using scatterometers, satellites, space shuttles, and airborne synthetic aperture radars (SAR) for many years. SAR data are well suited for estimating soil moisture due to the relationship of the dielectric constant and soil moisture. According to Ulaby et al. (1987), for a given soil condition (roughness or texture) radar backscatter is linearly dependent on volumetric moisture (m_v) in the upper 2 to 5 cm of soil with a correlation $R^2 \sim 0.8$ to 0.9.

In bare soil conditions, radar scattering is determined by surface roughness (geometry of the air soil boundary) and the microwave dielectric properties of the soil medium. The geometric factors affect the shape of the scattering pattern for an incident wave while the dielectric properties control the magnitude of reflection, absorption and transmission (Dobson and Ulaby, 1998). The average dielectric properties of the soil medium are dependent on the engineering properties of the soil including moisture content, density, texture, mineralogy and fluid chemistry. The dielectric constant of a material consists of two parts: real (ϵ') and imaginary (ϵ''). In case of a perfectly dry soil, the relative dielectric constant is independent of soil type (Dobson et al., 1985). Dielectric constant in liquid water shows strong dependence on the microwave frequency and weak sensitivity to physical temperature. When compared to dry soil the real part of the relative dielectric constant is 30 times greater and the imaginary part is about two orders of magnitude larger (Dobson and Ulaby, 1998). Due to the relationship between the dielectric constant in liquid water and microwave frequency the addition of water in liquid form to soil changes the dielectric constant of the mixture markedly.

The penetration depth into a soil by microwave is proportional to radar wavelength (Dobson and Ulaby, 1998). Significant penetration can occur in low loss materials, such as arid soils. Maximum penetration can occur in dry soil condition, whereas, the least penetration will occur in wet soils.

Studies, particularly in the past decade, have resulted in many methods, algorithms, and models relating satellite-based imagery from radar backscatter to surface soil moisture, however, no operational algorithm exists using radar data acquired by existing spaceborne sensors (Borgeaud and Saich, 1999). According to Moran et al. (2004) the promising approaches using SAR sensors for soil moisture estimation include: semi-empirical approaches, change detection, data fusion, and SAR with microwave scattering models.

Semi-empirical algorithms generally use SAR imagery of single wavelength, incident angle and polarization. Multiple passes and/or ancillary information are required for better accuracy. This approach is often scene or site dependent (Moran et al., 2000; Quesney et al., 2000). The change detection algorithms require multiple passes of SAR data and this approach has potential as an operational application (Engman, 1994). The reason for the operational suitability of this approach is that the algorithm is based on the assumption that the temporal variability of surface roughness and vegetation is at longer time scale than that of soil moisture content, and therefore, the change in radar backscatters between repeat passes results from the change in soil moisture. (Lu and Meyer, 2002). Research has been conducted into data fusion using passive and active microwave data, and microwave and optical data. Passive-active microwave data fusion algorithms use active backscattering coefficient to determine fine resolution vegetation biomass and surface roughness, and passive brightness temperature to estimate soil moisture content (Bindlish and Barros, 2002). The microwave-optical data fusion algorithms simplify the inverse problem for soil moisture content estimation on the basis of complementarily or interchangeability of optical and SAR data (Changey et al., 1995). Empirical, semi-empirical and theoretical microwave scattering models are available for use with the SAR data for soil moisture estimation. The Water Cloud Model (WCM) (Attema and Ulaby, 1978) and the Integral Equation Model

(IEM) (Fung et al., 1992; Colpitts, 1998) are common examples of this kind of models. The models are inverted to estimate soil moisture content from radar backscattering coefficient. Soil moisture estimation accuracy is higher by this approach, however, model parameterization is complex. These SAR based soil moisture estimation algorithms are described and explained in detail in Henderson and Lewis (1998) and in Moran et al. (2004).

1.3 Microwave Remote Sensing of Soil Moisture in Semi-arid Environment

The presence of vegetative cover introduces complexity into soil moisture mapping due to the interaction of the microwave energy with the vegetation and soil. Depending on the amount of vegetation present, its dielectric properties, height and geometry (size, shape and orientation of its component parts), the sensitivity of microwave backscatter to volumetric soil moisture may be significantly reduced. Previous studies indicate that in a semi-arid environment the influence of sparse vegetation on the linear relationship between radar backscatter and soil moisture is negligible or can be ignored (Thomas et al., 2004; Lin and Wood, 1993; and Dubois et al., 1995).

The research results presented in this chapter attempted to verify this concept in the semi-arid environment of southeastern New Mexico. This research also explores the non-linear relationship between soil moisture and radar backscatter, and investigates the impact of vegetation in soil moisture estimation using microwave imagery in this area.

2. Study Site

Nash Draw, located in part of the northeastern Chihuahua desert in southeastern New Mexico (Figure 2), is a karst valley that developed in response to subsurface dissolution of evaporites and subsidence of the overlying strata (Holt et al., 2005). It is a complex example of the localized effects of evaporite karst on surface topography, near-surface geology, and hydrology (Powers et al., 2006). Although this area is in a semi-arid environment, the vegetation pattern is not uniform. Nash Draw covers an area of 400 sq. km and a subset area of 225 sq. km was selected as the study site.

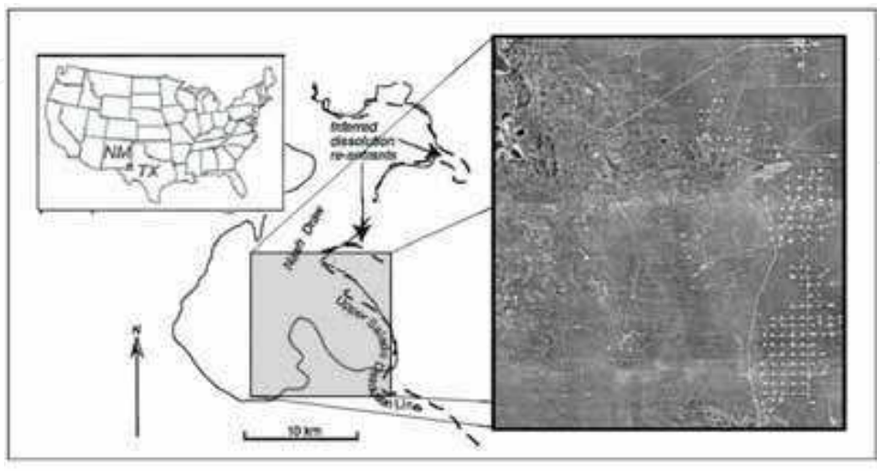

Fig. 2. Location of study site (Modified from Holt et al., 2005)

3. Data Used

Rainfall in Nash Draw is unreliable and erratic. Hydrologic data shows that August is commonly the wettest part of the season and October marks the end of the rainy season. It was assumed that imagery acquired during the months of August through November would record the maximum variation of soil moisture in the study site.

3.1 Synthetic Aperture Radar (SAR) Imagery

Due to its high spatial resolution, Radarsat 1 SAR Fine imagery was considered to be the best imagery for estimating soil moisture in the study site. The Alaska Satellite Facility (ASF) in Fairbanks, Alaska served as the Radarsat 1 data node for the United States. The ASF acquired 5 scenes of Radarsat 1 SAR Fine imagery covering the Nash Draw area for this research. The imagery was acquired at 10 m spatial resolution with 50 X 50 km swath coverage. The scenes were acquired in descending mode at 37 º incidence angle. The image acquisition dates include August 02 and 26, September 19, October 13 and November 06 of 2006. Figure 3 shows the acquired SAR imagery.

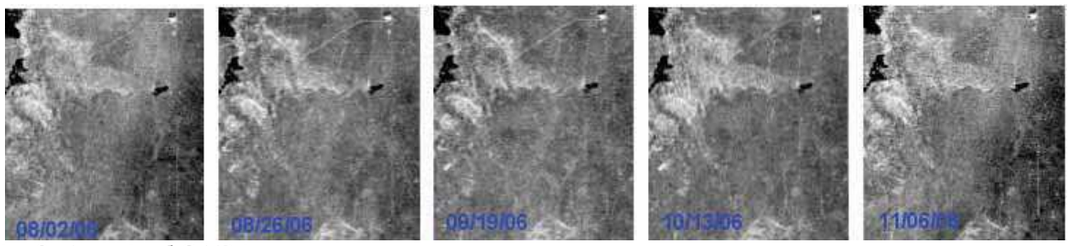

Fig. 3. Acquired SAR imagery

SAR Pre-processing

Initially all acquired SAR imagery were received as Level 0 products and then converted to level 1 products. These Level 1 SAR data have undergone several pre-processing phases including terrain correction, calibration and filtering to be ready for soil moisture estimation.

Data Calibration

An initial experiment was conducted using one radar scene to determine the suitability of σ^o or β^o for soil moisture estimation in our study site. It was found that backscatter values as β^o had a better correlation with field measured soil moisture than backscatter values as σ^o in our study site (Hossain and Easson, 2007). We believe that due to the low topographic relief in the study site variations in radar backscatter expressed as β^o produced better results. Based on these observations we decided to calibrate all the radar scenes as β^o for this project.

Removing Speckles

Coherent imaging systems produce images with a granular appearance, with a multitude of bright and dark spots caused by random constructive and destructive interference of the wavelets returning from the various scatterers within the resolution cell of the system (Goodman, 1975). From the mathematical point of view, the effect of this interference process can be regarded as a multiplicative noise, called speckle. In Synthetic Aperture

Radar (SAR) imagery, the presence of speckle affects the procedures for texture class discrimination. Speckle noise needs to be reduced to preserve edges and image texture (D'Elia et al., 2004). The most well known model used as the basis for the development of many of the existing speckle filters is the multiplicative model with an exponential probability density function (Touzi, 2002). To remove the speckles in the radar scenes we applied different types of filtering techniques with different window sizes. We found 5x5 Lee filtering provided better results and this method was used to de-speckle the acquired radar scenes.

Geometric Correction

The processed (calibrated and filtered) SAR data and the GIS coverage of the sample locations were georectified to the same projection system. All imagery and GIS data were georectified using recent aerial photograph and Universal Transverse Mercator (UTM) projection system.

3.2 Elevation Data

The knowledge of the local incident angle is essential for the quantitative estimation of soil moisture and roughness from SAR data. In the absence of topographic relief, the local incident angle equals the radar look angle. This is not true for terrain with larger topographic variations where the local incident angle becomes a function of the radar look angle and the local terrain slope. This makes the straightforward surface parameter estimation difficult (Hajnsek and Pottier, 2000). It is necessary to terrain correct the SAR data to allow geometric overlays of remotely sensed data from different sensors and/or geometries. The average elevation of the study site varies from 900 m to 1100 m, which is considered low relief for processing SAR imagery. However, despite the minimal topographic influence, a terrain correction was performed using USGS 30 m digital elevation model (DEM) to achieve greater geometric accuracy of the data.

3.3 Insitu Soil Moisture Data

Near-real time soil moisture data is needed to quantitatively map soil moisture with reasonable accuracy from SAR data. Soil samples were collected in selected parts of Nash Draw and analyzed to calculate volumetric soil moisture for calibration of the SAR imagery acquired on August 02, 2006 and November 06, 2006. Eighty soil samples were collected within a site covering 225 sq. km in Nash Draw.

Sampling Technique

A stratified soil sampling technique (Dane and Topp, 2002) was used in the acquisition of the soil samples. Using this method, the study site was divided into several grids and a simple random sampling technique was used in each grid with prior definition of sample size. The study site was divided into 4 equal parts and random sample points were selected in each part using a 500 m grid spacing, with 20 samples collected in each quadrant. Accessibility and variation in soil types was given preference for selecting sampling sites. Samples were collected for measuring volumetric soil moisture. Figure 4 shows the distribution of the collected soil sample locations in the study site.

RADARSAT 1 acquires imagery in HH polarization and in C band with 5.7 cm wavelength and 5.3 GHz frequency (RADARSAT International, 1995). The RADARSAT 1 beam should be able to penetrate the ground at least up to 3 cm in dry conditions. Therefore, sample collection was limited to within 3 cm below the land surface. A cylinder with 3 cm length and 5.7 cm diameter was used to collect soil cores. Figure 4 shows the procedure of soil sample collection.

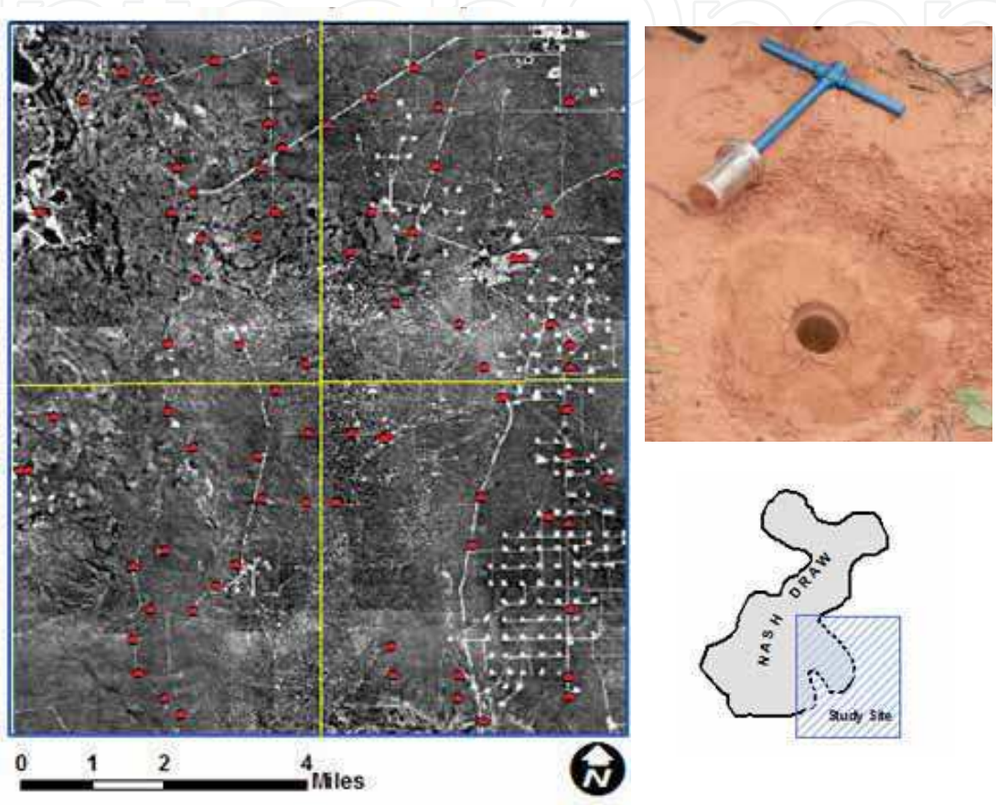

Fig. 4. Location and distribution of soil samples collected to measure the in situ soil moisture content (Left), and demonstration of soil sample collection (Right)

Volumetric Soil Moisture Measurement

Gravimetric soil moisture was measured and values were converted to volumetric soil moisture using sample volume. The ASTM D 2216-98 standard procedure (with modification) was used to calculate the gravimetric soil moisture and Equations (3) and (4) were used to calculate the volumetric moisture content.

$$w_v = \frac{V_w}{V} \times 100 \tag{3}$$

$$w_v = \frac{W_{ms} - W_{ds}}{76.55} \times 100 \tag{4}$$

Where, w_v = volumetric soil moisture (%), V_w = volume of moisture content (cc), V = volume of sample = 76.55 (cc), W_{ms} = weight of moist soil (gm), W_{ds} = weight of dry soil (gm), V_w = $W_{ms} - W_{ds}$ (volume of 1 gm water = 1 cc).

Soil moisture measurements for sample # 15 and sample # 115 were excluded from all analysis due to the proximity of these samples to a lake in the study area (Figure 5). Samples # 15 and # 115 had soil moisture measurements of 24.6% and 22.48%, respectively. Soil moisture measurements for samples # 31 and # 32 (from August data set) and for samples # 131 and # 132 (from November data set) were also excluded from the analysis due the distortion of SAR backscatter at these sample locations. These samples are located in dune sand and the backscatter values in the SAR imagery for that area are distorted apparently due to total reflection of the radar signal (Figure 6). Table 2. shows the statistics of the in situ soil moisture measurements.

Statistics	Measurement Dates	
	August 01-03, 2006	November, 04-06, 2006
Mean	6.48	2.80
Minimum	2.55	0.26
Maximum	14.53	10.16
St. Deviation	2.56	2.13

Table 2. Statistics of in situ soil moisture measurements

3.4 Vegetation Maps

Vegetative cover can strongly influence soil moisture mapping with SAR imagery due to the interaction of the microwaves with the vegetation and soil. The amount of vegetation, its dielectric properties and distribution pattern can significantly impact the sensitivity of microwave backscatter to volumetric soil moisture. A vegetation distribution map is needed for mapping soil moisture using SAR with reasonable accuracy.

A vegetation map for the study site was not available at the same resolution as the SAR imagery. The acquired SAR imagery was used to produce a time series of vegetation maps for the study site.

General Vegetation Distribution Pattern Map

We combined the acquired five radar scenes to produce a temporal data set [Figure 7(a)]. The temporal data set was then used to perform multi-temporal analysis to create a vegetation map of the study site. Vegetation signatures were obtained from the multi-temporal data for areas with little or no vegetation, sparse vegetation and dense vegetation. The obtained signatures were applied to the radar imagery to produce the vegetation map [Figure 7(b) and 7(c)]. Finally we simplified the vegetation map by dividing the study site into two zones: Zone 1 represents the area characterized by sparse, thin or no vegetation and Zone 2 represents areas characterized by comparatively denser vegetation [Figure 7(d)].

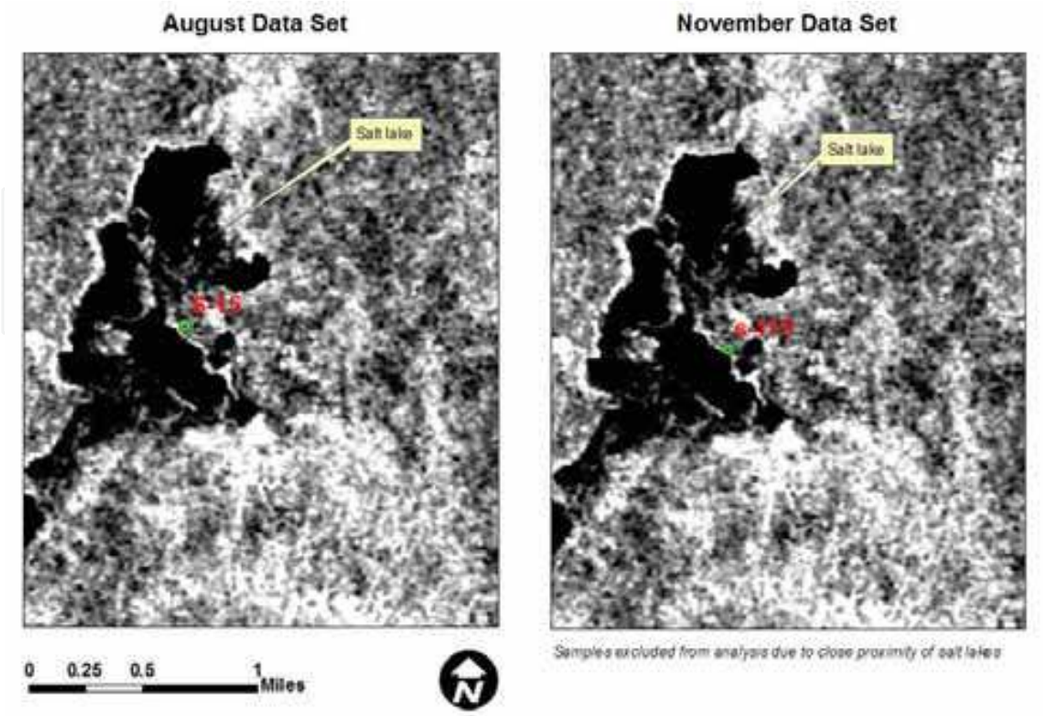

Fig. 5. Exclusion of samples # S-15 and S-115

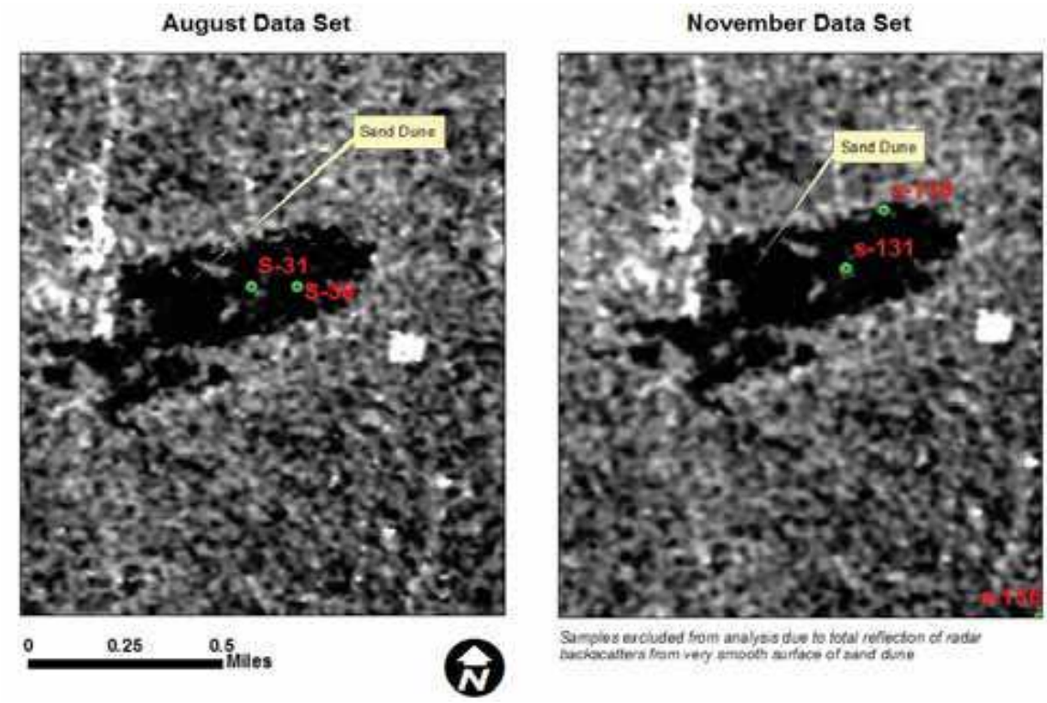

Fig. 6. Exclusion of samples # S-31, S-38, S-131 and S-138

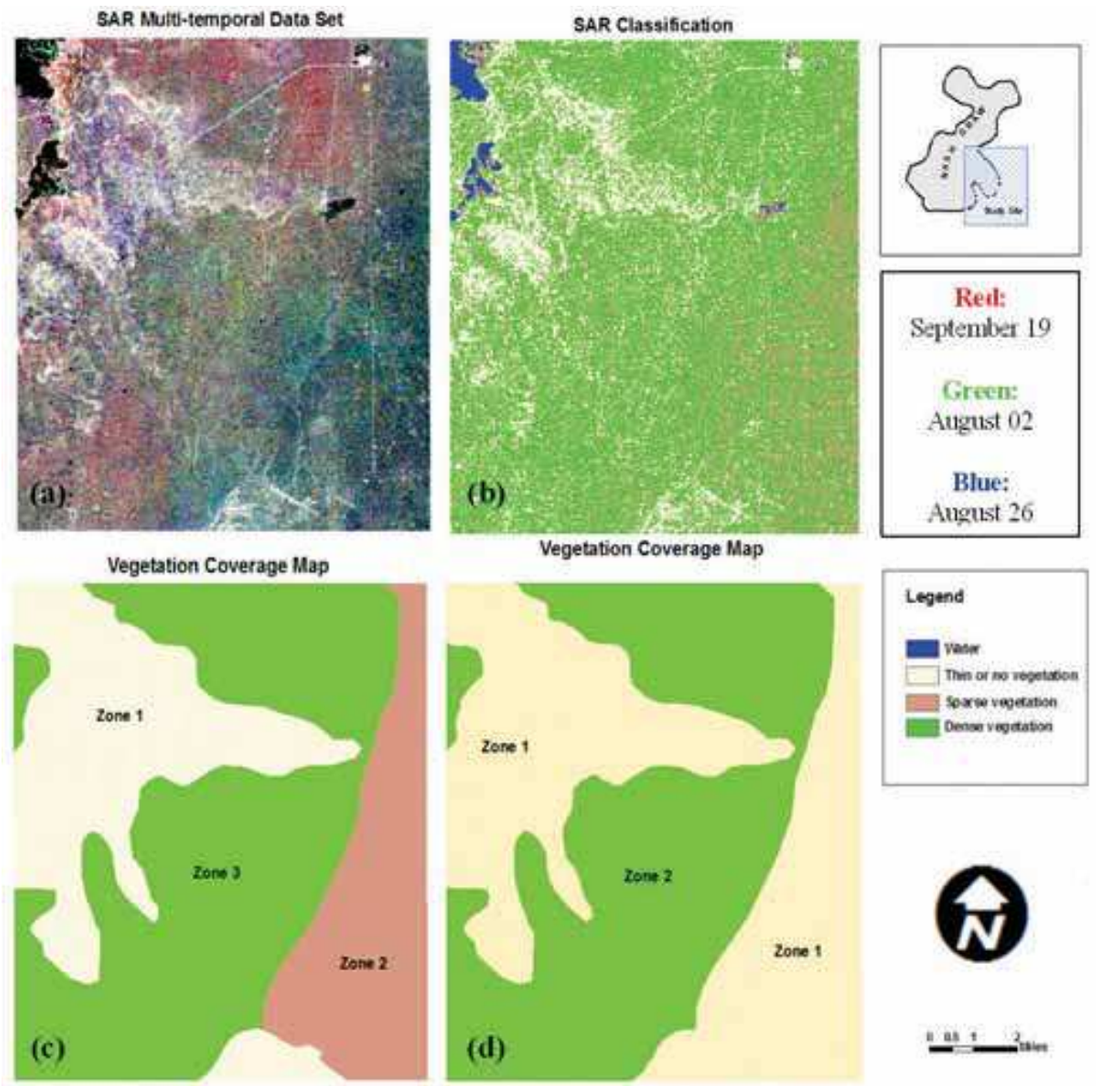

Fig. 7. Vegetation mapping

4. Methods

The algorithms developed by a semi-empirical approach are the most common and widely used (Moran et al., 2000). In this study simple linear regression was performed between soil moisture obtained from the field data and radar backscatter to study the linear relationship between radar reflectivity and soil moisture. An Artificial neural network (ANN) was used to study the non-linear relationship between radar backscatter (reflectivity) and soil moisture. Correlation coefficient (R^2) values were used to evaluate the suitability of the numerical models to map soil moisture in southeastern New Mexico

4.1 Simple Linear Regression

According to Ulaby et al. (1996), the radar backscatter from a surface with vegetation consists of three components: (1) product of the backscatter contribution of bare soil surface ($\sigma°$) and the two way attenuation of the vegetated layer (τ^2), (2) the direct backscatter contribution of the vegetation layer ($\sigma°_{dv}$), and (3) multiple scattering involving the vegetation elements and the ground surface ($\sigma°_{int.}$).

$$\sigma^\circ = \tau^2 \sigma_s^\circ + \sigma_{dv}^\circ + \sigma_{\text{int}}^\circ \tag{5}$$

In case of densely vegetated surface, $\tau^2 \sim 0$ and $\sigma°$ is determined largely by volumetric scattering from the vegetation canopy (Moran et al., 2004). For sparsely vegetated surfaces, $\tau^2 \sim 1$ and the second and third terms in the Equation (5) are negligible, and in this situation $\sigma°$ is determined by the soil roughness and moisture content (Moran et al., 2004). Therefore, for bare soil, $\sigma°_s$ has a functional relation with soil moisture, m_s and surface roughness, R (Engman and Chauhan, 1995), and it can be expressed as follows:

$$\sigma_s^\circ = f(R, m_s) \tag{6}$$

This indicates that for a target with uniform R, m_s can be estimated using the following expression:

$$m_s = a + b\sigma^\circ \tag{7}$$

Where a and b are regression coefficients, which are usually determined from field experiments encompassing the target-invariant R and the scene-invariants SAR wavelength (λ), incidence angle (θ_i), polarization, and calibration. However, Equation (7) is only valid for a given sensor, land use, and soil type, and for targets when τ^2, $\sigma°_{dv}$ and $\sigma°_{int}$ are known or negligible (Moran et al., 2004).

Quesney et al. (2000) resolved Equations (5)-(7) to derive soil moisture information from ERS SAR measurements over an agricultural watershed in France on the basis of a priori vegetation classification of the site and in situ soil moisture measurements. This study separated the areas with low vegetation biomass for soil moisture estimation.

Similarly, for a semiarid watershed in Arizona, Moran et al. (2000) utilized the difference between dry- and wet-season SAR $\sigma°$ ($\Delta\sigma°$) to normalize the effects of surface roughness and topography on ERS SAR measurements. Thoma et al. (2004) improved on this approach to minimize empiricism and used a quantitative form of $\Delta\ \sigma°$to map soil moisture for an entire watershed with RADARSAT for three dates in 2003. In these studies, the effects of sparse vegetation were found to be negligible and could be ignored. These observations were also supported with similar findings by Lin and Wood (1993), Chanzy et al. (1997), Demircan et al. (1993), Dobson et al. (1992), and Dubois et al. (1995).

Our study site, Nash Draw is characterized by a semi-arid environment and generally sparse vegetation cover. According to the previous researchers, the effects of sparse vegetation in the radar backscattering should be insignificant and can be ignored for soil

moisture estimation in this type of study site. It is important to note for our study site we modified the Equation (7) by using β^o instead of σ^o as the input of SAR reflectivity values.

$$m_s = a + b\beta^\circ \tag{8}$$

Radar β^o backscatter values were extracted for the soil sample locations where in situ soil moisture measurements were made and compared with volumetric soil moisture values for the sample locations. As discussed above, we used simple linear regression for the comparison and to calculate the coefficients *a* and *b* in the numerical model. We developed the model for the entire study site and also for different zones in the study site, based on vegetation density, to determine how well the model works for different land cover types, including vegetated areas and bare lands.

4.2 Non-Linear Regressions

Many SAR-based soil moisture estimation models assume that soil moisture distribution is linearly related to the radar reflectivity of the soil surface (e.g., Ulaby et al., 1996; Moran et al., 2000; Dobson et al.,1992; Dubois et al., 1995). Limited studies were conducted in the past to explore the non-linear relationship between soil moisture and radar backscatter (reflectivity). In this study we developed neural networks based numerical models to estimate soil moisture using SAR data in Nash Draw and to explore the non-linear relationship between soil moisture and SAR backscatter.

Artificial Neural Networks

Artificial neural networks, are a branch of artificial intelligence (Gardner and Dorling, 1998) in which the solution to a problem is learned from a set of examples (Bishop, 1994). A neural network can be regarded as a nonlinear mathematical function, which transforms a set of input variables into a set of output variables. The use of neural networks has been shown to be effective alternatives to more traditional statistical techniques (Schalkoff, 1992). Neural networks can be trained to approximate any smooth, measurable function (Hornik, et al., 1989), can model highly non-linear functions and can be trained to be accurately generalized when presented with unseen data (Gardner and Dorling, 1998). In a typical neural network model, a single neuron forms a weighted sum of the inputs $x_1, \ldots, x_d$ given by $a = S_i w_i x_i$, and then transforms this sum using a non-linear activation function $g(\ )$ to give a final output $z=g(a)$ (Figure 8).

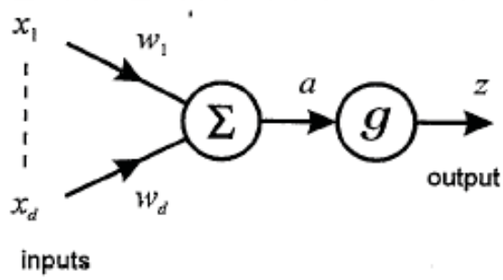

Fig. 8. A single processing unit in neural networks

A feed forward neural network can be regarded as a nonlinear mathematical function, which transforms a set of input variables into a set of output variables. The multilayer perceptron is the most widely used feed forward neural networks. Figure 8 shows a single processing unit of neural networks. If we consider a set of m such units, all with common inputs, then we arrive at a neural network having a single layer of adaptive parameters (weights). The output variables are denoted by z_j and are given by Equation (9).

$$z_j = g\left(\sum_{i=0}^{d} w_{ji} x_i\right) \tag{9}$$

Where w_{ji} is the weight for input i to j, and $g(\ )$ is an activation function as discussed previously.

The neural network model developed to estimate soil moisture in Nash Draw includes only one input, the radar backscatter values. This model demonstrates the nature of non-linear relationship between radar backscatter and soil moisture.

5. Results

5.1 Simple Linear regressions

The simple linear regression models for the entire study site are shown in Figure 9. Figure 10 shows the regression models for different vegetation zones for August, 2006 data set, and Figure 11 shows the regression models for different vegetation zones for November, 2006 data set. Equation (10) and Equation (11) represent the numerical models for the entire study site for August, 2006 data set and November 2006 data set respectively. Equation (12) and Equation (13) represent the numerical models for thinly vegetated areas (Zone 1) for August, 2006 data set and November 2006 data set respectively. Equation (14) and Equation (15) represent the numerical models for densely vegetated areas (Zone 2) for August, 2006 data set and November 2006 data set respectively. Table 3 shows the results of the regression models for August, 2006 and November, 2006 respectively.

$$m_{ss\_aug} = 18.47 + 0.82\beta^{\circ} \tag{10}$$

$$m_{ss\_nov} = 6.13 + 0.23\beta^{\circ} \tag{11}$$

$$m_{z1\_aug} = 27.4 + 1.34\beta^{\circ} \tag{12}$$

$$m_{z1\_nov} = 13.33 + 0.67\beta^{\circ} \tag{13}$$

$$m_{z2\_aug} = 4.11 - 0.11\beta^{\circ} \tag{14}$$

$$m_{z2\_nov} = 3.52 + 0.14\beta^{\circ} \tag{15}$$

Domain	Correlation Coefficient (R^2)	
	August 2006	November 2006
Entire study site	0.24	0.05
Thinly vegetated areas (Zone 1)	0.61	0.51
Densely vegetated areas (Zone 2)	0.01	0.04

Table 3. Regression results

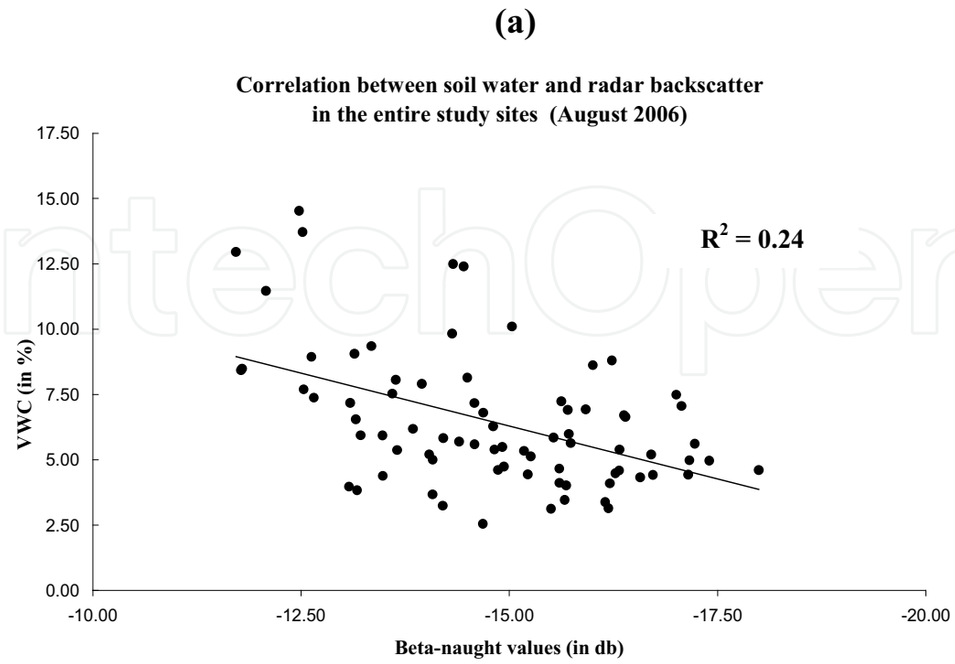

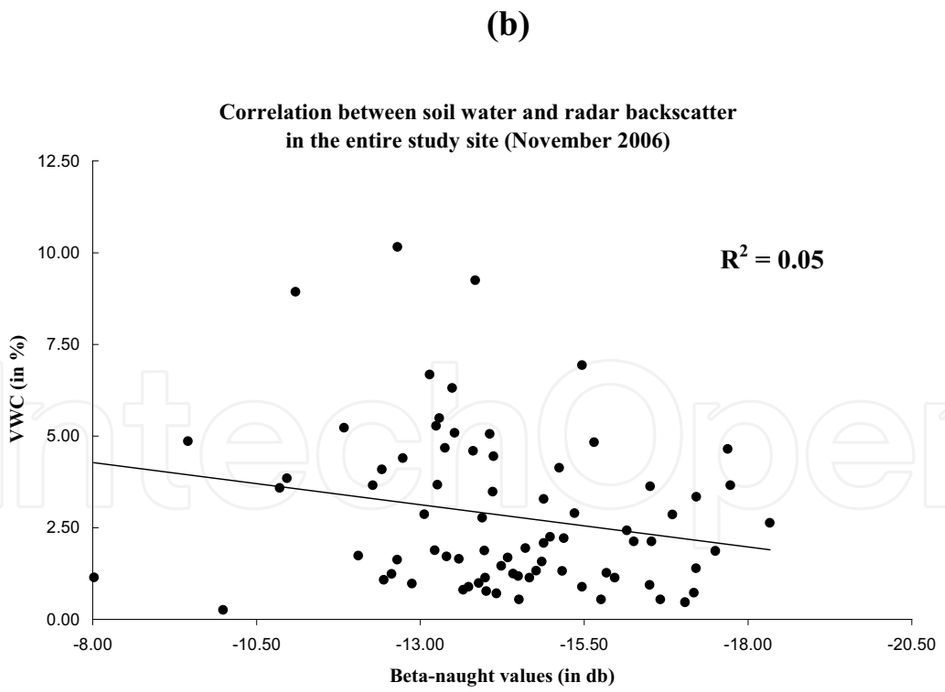

Fig. 9. Regression chart for entire study sites (a) August, 2006 and (b) November, 2006.

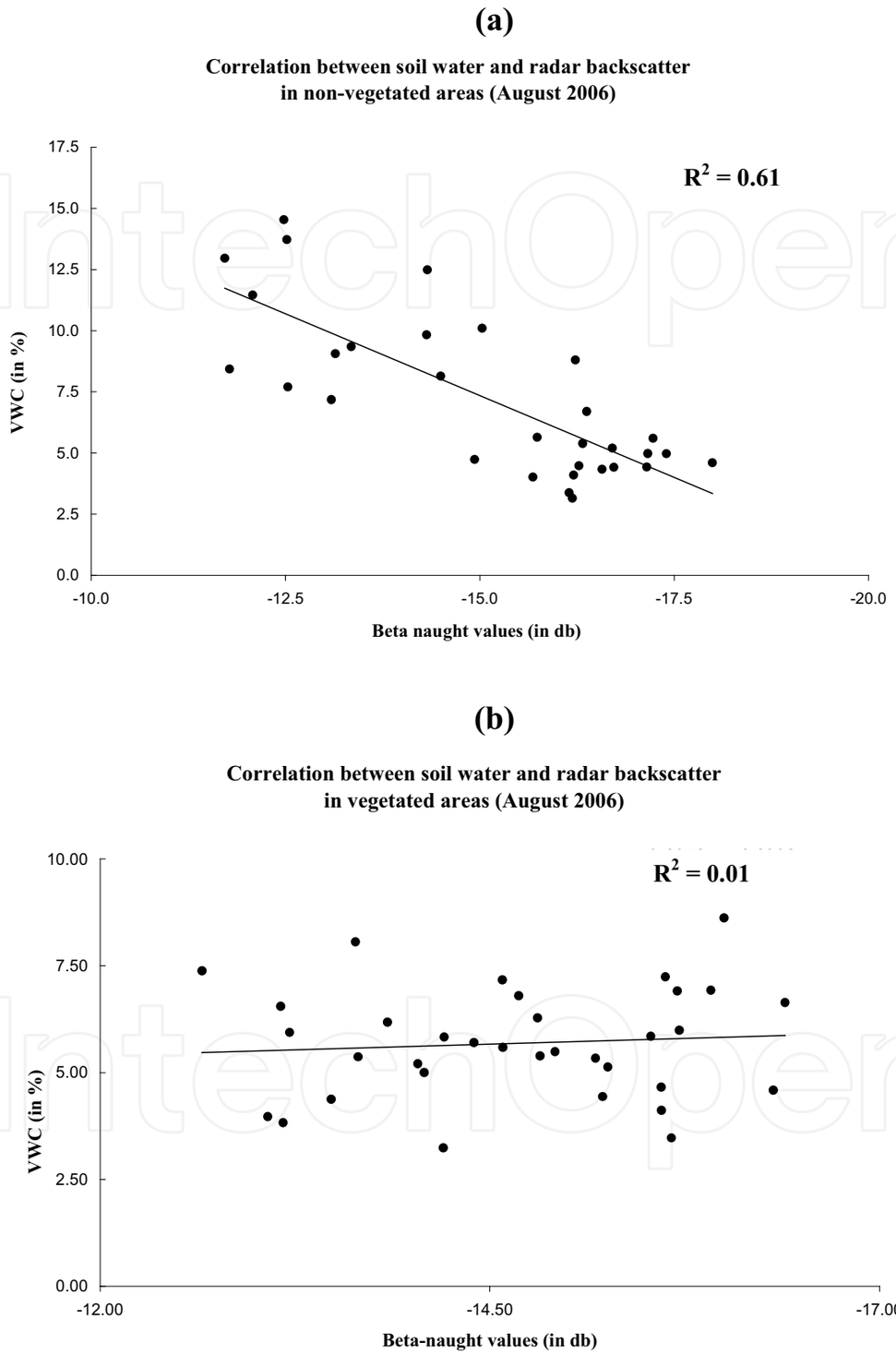

Fig. 10. Regression chart for different zones for August, 2006 data (a) Zone 1& (b) Zone 2 *(31 and 34 data values used in the analysis for zone 1 and Zone 2 respectively).*

(a)

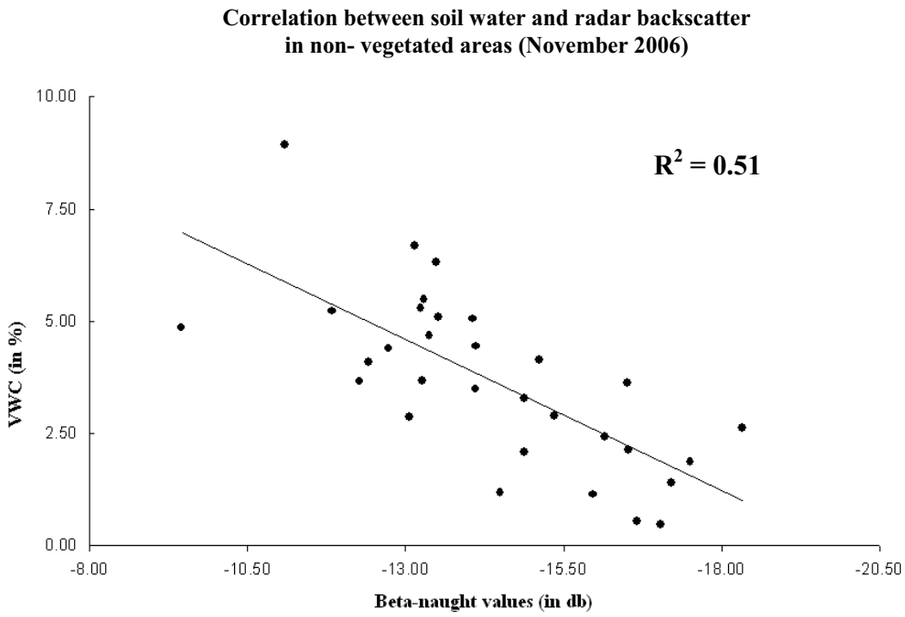

(b)

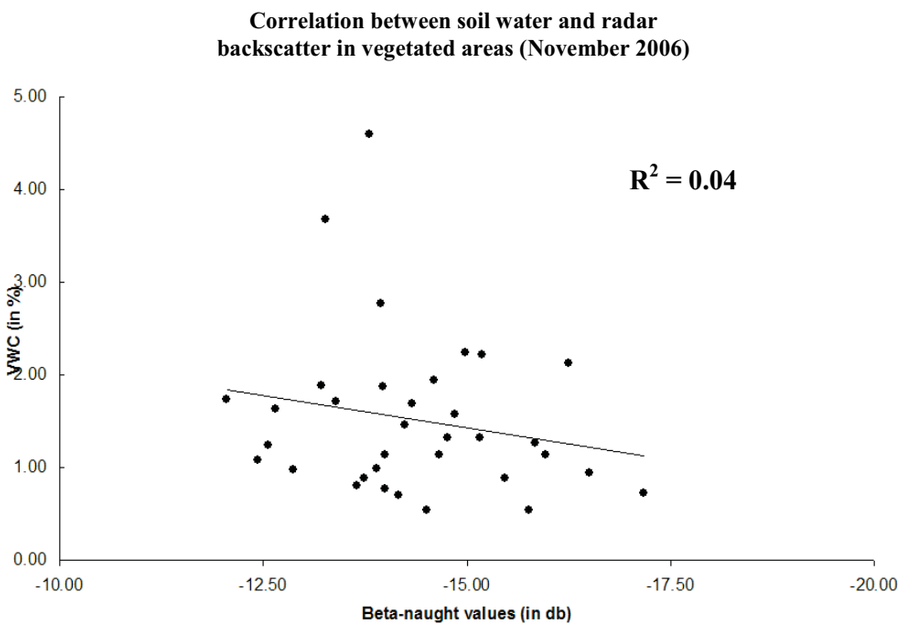

Fig. 11. Regression chart for different zones for November, 2006 data (a) Zone 1& (b) Zone 2 (*31 and 34 data values used in the analysis for zone 1 and Zone 2 respectively).*

The R^2 values of the numerical models developed for the entire study site indicate that the linear relationship between the radar backscatter values obtained for the entire study site and soil moisture is not well defined. We observed this for both the August (R^2 = 0.24) and November (R^2 = 0.05) data sets. The R^2 values of the numerical models developed for vegetated areas (Zone2) for both August and November data set are very low (0.01 and 0.04 respectively). We found higher R^2 values for the numerical models developed for non-vegetated or sparsely vegetated areas (Zone 1) for both August and November data set (0.61 and 0.51 respectively). These findings indicate that the relationship between radar backscatter and soil moisture in densely vegetated areas is not linear.

5.2 Non-linear Regressions (Neural Networks)

We developed neural network based non-linear numerical models for soil moisture estimation for the entire study site using the August data set. We developed models using radar backscatter values as the only input to investigate the non-linear relationship between the radar backscatter (reflectivity) and soil moisture. We used JMP 6.0 statistical software to perform the neural networks based analysis. The model correlation coefficient (R^2) and cross validation correlation coefficient (CV R^2) were used to evaluate the model performance for soil moisture prediction. A neural network with 3 hidden nodes resulted in correlation coefficient (R^2) and the cross validation correlation coefficient (CV R^2) of 0.24 and 0.11 respectively. This result indicates that the non-linear relationship between radar backscatter and soil moisture is also not well defined for the entire study site.

5.3 Model Evaluation

We evaluated the correlation coefficients (R^2) and cross validation correlation coefficients (CV R^2) (for the neural networks based models) developed by both linear and non-linear regressions for soil moisture estimation in Nash Draw, NM and made the following observations.

- Simple linear regression between radar backscatter values and in situ soil moisture measurements can be used to develop SAR based soil moisture estimation model with model R^2 values of 0.51 to 0.61, but the model application should be restricted to non-vegetated to thinly vegetated areas.
- Neural network based non-linear regressions using radar backscatter values and in situ soil moisture measurements can be used to develop soil moisture estimation model for the entire study site with a model R^2 value of 0.24 and CV R^2 of 0.11.

6. Conclusions and Discussion

Earlier researchers reported that in a semi-arid environment with sparse vegetation, there is a linear relationship between soil moisture and radar backscatter. Our research shows that in semi-arid environment the influence of vegetation can influence the accuracy of the soil moisture estimation using the linear relationship between the radar backscatter and soil moisture. This observation is supported by the lower R^2 values (0.24 – August data set and 0.05 – November data set) obtained for the numerical models developed for the entire study site, the higher R^2 values (0.61 – August data set and 0.51 – November data set) obtained for

the numerical models developed for the parts of the study site identified as very thin or sparsely vegetated areas, and very low R^2 values (0.01 – August data set and 0.04 – November data set) obtained for the numerical models developed for the parts of the study site identified as more densely vegetated areas.

The non-linear relationship between radar reflectivity and soil moisture was investigated using a numerical model developed by feed forward neural networks with radar backscatter values and near real time in situ soil moisture measurements. The model was developed for the entire study site and did not show a strong non-linear relationship between radar backscatter (reflectivity) and soil moisture. The correlation coefficient (R^2) (0.24) did not improve from that obtained by simple linear regression (0.24) between radar backscatter and soil moisture.

This research indicates that in semi-arid environment vegetation coverage can significantly reduced the accuracy of soil moisture estimation and mapping using numerical models based on simple linear and non-linear relationships between radar backscatter values derived from high resolution SAR imagery and near real time in situ soil moisture measurements. This research also shows that numerical models based on only radar backscatter and near real time in situ soil moisture measurements can only be used in thinly vegetated to bare soil conditions in a semi-arid environment to estimate and map soil moisture with improved accuracy (R^2 = 0.51 to 0.61).

We recommend to include soil type, soil salinity and surface elevation information (in addition to vegetation coverage and in situ soil moisture measurements) in both linear and non-linear numerical models to improve the accuracy of SAR based soil moisture estimation in semi-arid environment without separating the vegetated and non-vegetated zones.

7. Acknowledgements

Thanks are due to the NASA Applied Sciences Program and the University of Mississippi Geoinformatics Center (UMGC) for funding the project through a Rapid Prototyping Capability (RPC) for Earth-Sun Systems Sciences project at The University of Mississippi. Thanks are also due to the Alaska Satellite Facility (ASF) for providing the SAR imagery; Dr. Dennis Powers, Glen Garrett and Dirk O'Daniel for their assistance in the field to acquire soil samples for soil moisture analysis; and Patrick Yamnik for assisting in image processing and GIS analysis.

8. References

ASTM (Designation: D 2216 – 98). (1999). *Standard test method for laboratory determination of water (moisture) content of soil and rock by mass* (reprinted from the annual book of ASTM standards), American Society for Testing and Materials, 100 Barr Harbor Dr., West Conshohocken, PA 19428, 5p.

Attema, E. & Ulaby, F. (1978). Vegetation modeled as a water cloud, *Radio Science*, vol. 13, pp. 357–364, ISSN: 0048–6604.

Baghdadi, N; Holah, N. & Zribi, M. (2006). Soil moisture estimation using multi-incidence and multi-polarization ASAR data, *International Journal of Remote Sensing*, vol. 27, no. 9-10, pp. 1907-1920, ISSN: 1366-5901.

Bishop, C. M. (1994). Neural networks and their applications, *Review of Scientific Instruments.*, vol. 65, no. 6, pp. 1803-1833, ISSN: 0034-6748.

Bindlish, R. & Barros, A.P. (2001). Parameterization of vegetation backscatter in radar-based soil moisture estimation, *Remote Sensing of Environment*, vol. 76, no. 1, pp. 130–137, ISSN: 0034-4257.

Borgeaud, M. & Saich, P. (1999). Status of the retrieval of bio- and geophysical parameters from SAR data for land applications, *Proceedings of the International Geoscience and Remote Sensing Symposium, IGARSS '1999*, 28 June – 02 July, 1999, Hamburg, Germany, pp. 1901–1903.

Carlson, T.N.; Gillies, R.R. & Schmugge, T.J. (1995). An interpretation of NDVI and radiant surface temperature as measures of surface soil water content and fractional vegetation cover, *Agricultural and Forest Meteorology*, vol. 77, no. 3-4, pp. 191-205, ISSN: 0168-1923.

Chanzy, A.; Bruckler, L. & Perrier, A. (1995). Soil evaporation monitoring: a possible synergism of microwave and infrared remote sensing, *Journal of Hydrology*, vol. 165, no. 1-4, pp. 235–259, ISSN: 0022-1694.

Chanzy, A.; Kerr, Y.; Wigneron, J.P. & Calvet, J.C. (1997). Soil moisture estimation under sparse vegetation using microwave radiometry at C-band, *Proceedings of the International Geoscience and Remote Sensing Symposium, IGARSS '1997*, 3–8 August 1997, Singapore, pp. 1090–1092.

Colpitts, B.G. (1998). The integral equation model and surface roughness signatures in soil moisture and tillage type determination, *IEEE Transactions on Geoscience and Remote Sensing*, vol. 36, no. 3, pp. 833–837, ISSN: 0196-2892.

Dane, J. H. & Topp, G. C. (2002). *Methods of soil analysis*, *Part 4, Physical Methods, SSSA Book Series, No. 5*, 1692p, ISBN 0-89118-841-X.

D'Elia C.; Ferraiuolo, G.; Pascazio, V. & Schirnzi, G. (2004). An MRF based technique for speckle reduction in SAR images, *Proceedings of the International Geoscience and Remote Sensing Symposium,* IGARSS, 2004, 20-24 September 2004, Anchorage, AK, vol. 6, pp. 4211- 4214.

Demircan, A.; Rombach, M. & Mauser, W. (1993). Extraction of soil moisture from multitemporal ERS-1 SLC data of the Freiburg test site, *Proceedings of the International Geoscience and Remote Sensing Symposium, IGARSS '1993*, 18–21 August 1993, Tokyo, Japan, vol. 4, pp. 1794–1796.

Dobson, M. C. & Ulaby, F. T. (1998). Mapping soil moisture distribution with imaging radar. In: *Principles & Applications of Imaging Radar, Manual of Remote Sensing, 3rd Edition, Volume 2*, Henderson, F. M. & Lewis, A. J., pp. 407-433, John Wiley & Sons, Inc., ISBN: 0-471-29406-3, New York.

Dobson, M. C.; Ulaby, F. T.; El-Rayes M. & Hallikainen. (1985). Microwave dielectric behavior of wet soil, part II: four component dielectric mixing model, *IEEE Transaction on Geoscience and Remote Sensing,* vol. GE-24, no. 1, pp. 517-526, ISSN: 0196-2892.

Dobson, M.C. ; Pierce, L.; Arabandi, K.; Ulaby, F.T. & Sharik, T. (1992). Preliminary analysis of ERS-1 SAR for forest ecosystem studies, *IEEE Transactions on Geoscience and Remote Sensing*, vol. 30, pp. 203–21, ISSN: 0196-2892.

Dubois, P.C.; van Zyl, J. & Engman, E.T. (1995). Measuring soil moisture with imaging radars, *IEEE Transactions on Geoscience and Remote Sensing*, vol. 33, pp. 915–926, ISSN: 0196-2892.

Engman, E.T. (1994). The potential of SAR in hydrology, *Proceedings of the International Geoscience and Remote Sensing Symposium, IGARSS '94*, 8–12 August 1994, Pasadena, Calif. IEEE, Piscataway, N.J. pp. 283–285.

Engman, E.T. & Chauhan, N. (1995). Status of microwave soil moisture measurements with remote sensing, *Remote Sensing of Environment*, vol. 51, pp. 189-198, ISSN: 0034-4257.

Farnsworth R.K.; Barret E.C. & Dhanju M.S. (1984). *Application of remote sensing to hydrology including ground water*, IHP-II Project A. 1.5, UNESCO, Paris, France.

Fung, A.K.; Li, Z. & Chen, K.S. (1992). Backscattering from a randomly rough dielectric surface, *IEEE Transactions on Geoscience and Remote Sensing*, vol. 30, pp. 356–369, ISSN: 0196-2892.

Gardner, M.W. & Dorling, S.R. (1998). Artificial Neural Networks (The Multilayer Perceptron) - a review of applications in the atmospheric sciences, *Atmospheric Environment*, vol. 32, no. 14/15, pp. 2627-2636, ISSN: 1352-2310.

Georgakakos, K. P. & Baumer, O. W. (1996). Measurement and utilization of on-site soil moisture data, *Journal of Hydrology*, vol. 184, pp. 131–152, ISSN: 0022-1694.

Gillies, R. R.; Carlson, T. N.; Cui, J.; Kustas, W. P. & Humes, K. S. (1997). A verification of the 'triangle' method for obtaining surface soil water content and energy fluxes from remote measurements of the Normalized Difference Vegetation Index and surface radiant temperature, *International Journal of Remote Sensing*, vol. 18, pp. 3145–3166, ISSN: 0143-1161.

Glenn, N. F. & Carr, J. R. (2004). Establishing a relationship between soil moisture and RADARSAT-1 SAR data obtained over the Great Basin, Nevada, U.S.A., *Canadian Journal of Remote Sensing*, vol. 30, no. 2, pp.176–181, ISSN: 0143-1161.

Goodman, J. W. (1975). *Statistical properties of laser speckle patterns, in laser speckle and related phenomena*, Edited by J. C. Dainty, Springer, 1975, pp. 9-75.

Guindon, B. (1990). Development of a shape-from-shading technique for the extraction of topographic models from individual spaceborne SAR images, *IEEE Transactions on Geoscience and Remote Sensing,* vol. 28 no. 4, pp. 654–661, ISSN: 0196-2892.

Hajnsek, I. & Pottier E. (2000). Terrain correction for quantitative moisture and roughness retrieval using polarimetric SAR data, *Proceedings of the International Geoscience and Remote Sensing Symposium IGARSS 2000*, vol. 3, pp. 1307-1309.

Henderson, F. M. & Lewis, A. J. (1998). *Principles & Applications of Imaging Radar, Manual of Remote Sensing, 3rd Edition, Volume. 2*, pp. 01-07, John Wiley & Sons, Inc., ISBN: 0-471-29406-3, New York.

Holt, R.M.; Beauheim, R.L.& Powers, D.W. (2005). Predicting fractured zones in the Culebra Dolomite, In: Faybishenko, B., Witherspoon, P.A., and Gale, J., eds., Dynamics of Fluids and Transport in Fractured Rock: *AGU Geophysical Monograph Series*, vol. 162, p. 103-116, ISSN 0065-8448.

Hornik, K.; Stinchcombe, M. & White, H. (1989). Multilayer feed forward networks are universal approximators, *Neural Networks*, vol. 2, pp. 259-366, ISSN: 0893-6080.

Hossain, F. & Anagnostou, E.N. (2005). Numerical investigation of the impact of uncertainties in satellite rainfall and land surface parameters on simulation of soil moisture, *Advances in Water Resources,* vol. 28, no. 12, pp. 1336-1350, ISSN**:** 0309-1708.

Hossain, A. & Easson, G. (2008). Evaluating the potential of VI-LST Triangle Model for quantitative estimation of soil moisture using optical imagery, *Proceedings of the International Geoscience and Remote Sensing Symposium IGARSS 2008*. IEEE International, vol. 3, issue, 7-11 July 2008, pp. 879 – 882.

Hossain, A. & Easson, G. (2006). Mapping spatial variation in surface moisture using reflective and thermal ASTER imagery for Southern Africa, *ASPRS 2006 Annual Conference*, Reno, Nevada, May 1-5, 2006.

Hossain, A.; Easson, G.; Powers, D. W. & Holt, R. M. (2007). Impact of variation in reflectivity of microwave data for soil moisture estimation in semi-arid environment, *Sigma Xi Poster Presentation*, The University of Mississippi, University, MS.

Jackson, T. J. (2002). Remote sensing of soil moisture: implications for groundwater recharge, *Hydrogeology Journal*, vol. 10, pp. 40-51, ISSN: 1431-2174.

Kelly R. E. J.; Davie T. J. A. & Atkinson P. M. (2003). Explaining temporal and spatial variation in soil moisture in a bare field using SAR imagery, *International Journal of Remote Sensing*, vol. 24, no. 15, pp. 3059-3074, ISSN: 0143-1161.

Lambin, E. F. & Ehrlich, D. (1996). The surface temperature-vegetation index space for land cover and land-cover change analysis, *International Journal of Remote Sensing*, vol. 17, pp.1087-1105, ISSN: 0143-1161.

Lin, D.S. & Wood, E.F. (1993). Behavior of AirSAR signals during MACEurope '91, Proceedings *of the International Geoscience and Remote Sensing Symposium, IGARSS '1993*, 18–21 August 1993, Tokyo, Japan, vol. 4, pp. 1800–1802.

Lu, Z., & Meyer, D.J. (2002). Study of high SAR backscattering caused by an increase of soil moisture over a sparsely vegetated area: implications for characteristics of backscatter, *International Journal of Remote Sensing*, vol. 23, pp. 1063–1074, ISSN: 0143-1161.

Meijerink, A. M. J.; Schultz G. A. & Engman, E. T. (eds.). (2000). Remote sensing in hydrology and water management, Springer, Berlin Heidelberg New York, pp 305–325.

Moran, S. M.; Clarke, T. R.; Inoue, Y. & Vidal, A. (1994). Estimating crop water deficit using the relationship between surface-air temperature and spectral vegetation index, *Remote Sensing of Environment*, vol. 49, pp. 246-263, ISSN: 0034-4257.

Moran, M.S.; Hymer, D.C.; Qi, J. & Sano, E.E. (2000). Soil moisture evaluation using multi-temporal Synthetic Aperture Radar (SAR) in semiarid rangeland, *Agricultural and Forest Meteorology*, vol. 105, pp. 69–80, ISSN: 0168-1923.

Moran, S. M.; Christa D.; Peters, L.; Watts J. M. & McElroy, S. (2004). Estimating soil moisture at the watershed scale with satellite-based radar and land surface models, *Canadian Journal of Remote Sensing*, vol. 30, no. 5, pp. 805–826, ISSN: 1712-7971.

Nemani, R. & Running, S., 1993, Developing satellite derived estimates of surface moisture status, *Journal of Applied Meteorology*, vol. 32, pp. 548-557, ISSN: 1558-8424.

Powers, D.W.; Beauheim, R.L.; Holt, R.M. & Hughes, D.L. (2006). Evaporite karst features and processes at Nash Draw, Eddy County, New Mexico, In: Caves & Karst of Southeastern New Mexico, Land, L. and others, eds., *NM Geological Society Fifty-seventh Annual Field Conference Guidebook*, pp. 253-266, ISBN: 1-58546-092-3 (ISSN: 0077-8567).

Quesney, A.; Le Hégarat-Mascle, S.; Taconet, O.; Vidal-Madjar, D; Wigneron, J.P.; Loumagne, C. & Normand, M. (2000). Estimation of watershed soil moisture index from ERS/SAR data, *Remote Sensing of Environment*, vol. 72, pp. 290–303, ISSN: 0034-4257.

RADARSAT International, 1995, RADARSAT Illuminated: your guide to products and services, Unpublished manual, 60p.

Rayleigh, J.W. S. & Robert B. L. (1945). *The theory of sound*, vol. 1, ISBN: 0-486-60292-3, New York.

Raney, R. K. (1998). Radar fundamentals: Technical perspective. In: *Principles & Applications of Imaging Radar, 3rd Edition, Volume 2*, Henderson, F. M. & Lewis, A. J., pp. 407-433, John Wiley & Sons, Inc., ISBN: 0-471-29406-3, New York.

Robock; Alan; Lifeng, L.; Eric, F. W.; Fenghua W.; Kenneth, E.; Mitchell; Paul, R. H.; John C. S.; Dag L.; Brian C.; Justin S.; Qingyun D.; Wayne H.; Rachel T. P.; Dan T. J.; Jeffrey B. B. & Kenneth C. C. (2003). Evaluation of the North American Land Data Assimilation System over the Southern Great Plains during the warm season, *Journal of Geophysical Research*, vol. 108 (D22), no. 8846, ISSN: 0148–0227.

Schalkoff, R. (1992). Pattern recognition: Statistical, structural and neural approaches, John Wiley and Sons, New York.

Schneider, K., & Oppelt, N. (1998). The determination of mesoscale soil moisture patterns with ERS data, In *Proceedings of the International Geoscience and Remote Sensing Symposium, IGARSS '98*, 6–10 July 1998, Seattle, Wash. IEEE, New York. pp. 1831–1833.

Thoma, D. P.; Moran, M. S.; Bryant, R.; Rahman, M.; Holifield-Collins, C. D.; Skirvin, S.; Sano, E. E. & Slocum, K. (2006). Comparison of four models to determine surface soil moisture from C-band radar imagery in a sparsely vegetated semiarid landscape, *Water Resources Research*, vol. 42, pp. 1-12, ISSN: 0043–1397.

Touzi R. (2002). A review of speckle filtering in the context of estimation, theory, *IEEE Transactions on Geoscience And Remote Sensing*, vol. 40, pp. 2392-2404, ISSN: 0196-2892.

Ulaby, F.T.; Moore, M. K. & Fung, A.K. (1986). *Microwave remote sensing, active and passive, from theory to application, Volume 3*, Artech House, ISBN: 0-89006-192-0. Norwood, MA

Ulaby, F.T.; Held, D.; Donson, M.C. & McDonald, K.C. (1987). Relating polarization phase difference of SAR signals to scene properties, *IEEE Transactions on Geoscience and Remote Sensing,* vol. GE-25, pp. 83-92, ISSN: 0196-2892.

Ulaby, F.T.; Dubois, P.C. & Van Zyl, J. (1996). Radar mapping of surface soil moisture, *Journal of Hydrology*, vol. 184, pp. 57–84, ISSN**:** 0022-1694.

IntechOpen

Geoscience and Remote Sensing

Edited by Pei-Gee Peter Ho

ISBN 978-953-307-003-2
Hard cover, 598 pages
Publisher InTech
Published online 01, October, 2009
Published in print edition October, 2009

Remote Sensing is collecting and interpreting information on targets without being in physical contact with the objects. Aircraft, satellites ...etc are the major platforms for remote sensing observations. Unlike electrical, magnetic and gravity surveys that measure force fields, remote sensing technology is commonly referred to methods that employ electromagnetic energy as radio waves, light and heat as the means of detecting and measuring target characteristics. Geoscience is a study of nature world from the core of the earth, to the depths of oceans and to the outer space. This branch of study can help mitigate volcanic eruptions, floods, landslides ... etc terrible human life disaster and help develop ground water, mineral ores, fossil fuels and construction materials. Also, it studies physical, chemical reactions to understand the distribution of the nature resources. Therefore, the geoscience encompass earth, atmospheric, oceanography, pedology, petrology, mineralogy, hydrology and geology. This book covers latest and futuristic developments in remote sensing novel theory and applications by numerous scholars, researchers and experts. It is organized into 26 excellent chapters which include optical and infrared modeling, microwave scattering propagation, forests and vegetation, soils, ocean temperature, geographic information , object classification, data mining, image processing, passive optical sensor, multispectral and hyperspectral sensing, lidar, radiometer instruments, calibration, active microwave and SAR processing. Last but not the least, this book presented chapters that highlight frontier works in remote sensing information processing. I am very pleased to have leaders in the field to prepare and contribute their most current research and development work. Although no attempt is made to cover every topic in remote sensing and geoscience, these entire 26 remote sensing technology chapters shall give readers a good insight. All topics listed are equal important and significant.

How to reference

In order to correctly reference this scholarly work, feel free to copy and paste the following:

A. K. M. Azad Hossain and Greg Easson (2009). Microwave Remote Sensing of Soil Moisture in Semi-arid Environment, Geoscience and Remote Sensing, Pei-Gee Peter Ho (Ed.), ISBN: 978-953-307-003-2, InTech, Available from: http://www.intechopen.com/books/geoscience-and-remote-sensing/microwave-remote-sensing-of-soil-moisture-in-semi-arid-environment

INTECH
open science | open minds

InTech Europe
University Campus STeP Ri
Slavka Krautzeka 83/A

InTech China
Unit 405, Office Block, Hotel Equatorial Shanghai
No.65, Yan An Road (West), Shanghai, 200040, China

www.intechopen.com

51000 Rijeka, Croatia
Phone: +385 (51) 770 447
Fax: +385 (51) 686 166
www.intechopen.com

中国上海市延安西路65号上海国际贵都大饭店办公楼405单元
Phone: +86-21-62489820
Fax: +86-21-62489821

IntechOpen

IntechOpen